

Numerical computations of next-to-leading order corrections in spinfoam large- j asymptotics

Muxin Han^{1,2} Zichang Huang^{4,5} Hongguang Liu^{2,3} Dongxue Qu¹

¹*Department of Physics, Florida Atlantic University, 777 Glades Road, Boca Raton, FL 33431-0991, USA*

²*Institut für Quantengravitation, Universität Erlangen-Nürnberg, Staudtstr. 7/B2, 91058 Erlangen, Germany*

³*Center for Quantum Computing, Pengcheng Laboratory, Shenzhen 518066, China*

⁴*Department of Physics, Center for Field Theory and Particle Physics, and Institute for Nano- electronic devices and Quantum computing, Fudan University, Shanghai 200433, China*

⁵*State Key Laboratory of Surface Physics, Fudan University, Shanghai 200433, China*

E-mail: dqu2017@fau.edu

ABSTRACT: The next-to-leading order correction is studied numerically in the large- j expansion of the Lorentzian Engle-Pereira-Rovelli-Livine (EPRL) 4-simplex amplitude. We perform large- j expansions of Lorentzian EPRL 4-simplex amplitudes with two different types of boundary states: coherent intertwiners and the coherent spin-network, and we numerically compute leading order and next-to-leading $O(1/j)$ contributions of these amplitudes. Dependences of their $O(1/j)$ corrections on the Barbero-Immirzi parameter γ are studied, and we show that they, as functions of γ , stabilize to finite real constants as $\gamma \rightarrow \infty$. In addition, we obtain quantum corrections to the Regge action from the $O(1/j)$ contribution of the spinfoam amplitude.

Contents

1	Introduction	1
2	EPRL 4-simplex amplitude	3
3	Boundary data and critical point	5
3.1	Boundary data	5
3.2	Critical points	7
4	Next-to-leading order correction in large-j 4-simplex amplitude with coherent-intertwiner boundary state	8
4.1	Explicit expression of 4-simplex amplitude	8
4.2	Asymptotic expansion and next-to-leading order correction	9
4.3	Numerical results	11
5	Next-to-leading order correction in large-j 4-simplex amplitude with coherent spin-network boundary state	13
5.1	Coherent spin network state	13
5.2	Numerical results	15
6	Conclusion	17
A	The $SL(2, \mathbb{C})$ Haar measure	18

1 Introduction

Loop Quantum Gravity (LQG) is a candidate of background-independent and non-perturbative quantum theory of gravity [1–3]. Spinfoam model is a covariant approach of Loop Quantum Gravity and formulates LQG transition amplitude, called the spinfoam amplitude, as a sum-over-history of quantum geometries [4, 5]. The Lorentzian Engle-Pereira-Rovelli-Livine (EPRL) model [6] is one of successful spinfoam models, due to its simplicity and semiclassical behavior [7–9]. In the Lorentzian EPRL model, the spinfoam amplitude can be described by a path integral representation that has been employed in studying the large- j asymptotic behavior, which is related to the Regge action of classical discrete gravity [10, 11]. Computing spinfoam amplitudes is the central task in developing the spinfoam formulation of LQG, especially in the perspective of extracting quantum corrections to classical gravity. An efficient tool of computing the Lorentzian EPRL spinfoam amplitude is the large- j asymptotic expansion, which has been extensively applied to the semiclassical analysis of spinfoam models. However existing studies on the Lorentzian EPRL model mainly focus on the leading order contribution in the large- j asymptotics, while higher order corrections have not been explored. Higher order corrections in the large- j expansion are expected to relate to quantum-gravity effects in LQG, while the leading order relates to the semiclassical limit.

The purpose of this work is to study the next-to-leading order correction in the large- j expansion of the Lorentzian EPRL 4-simplex amplitude. We perform large- j expansions of Lorentzian EPRL 4-simplex amplitudes with two different choices of boundary states: coherent-intertwiners [12] and the coherent spin network [13–17], and we numerically compute leading order and next-to-leading

$O(1/j)$ contributions of these amplitudes. We also study the dependences of their $O(1/j)$ corrections on the Barbero-Immirzi parameter γ . As a functions of γ , $O(1/j)$ corrections stabilize to finite real constants as $\gamma \rightarrow \infty$. As a result, the quantum correction to the Regge action can be obtained from our computation.

Here we introduce main results of this paper: We consider the same Lorentzian nondegenerate 4-simplex geometry and boundary data as in [18] and construct spinfoam critical points of the EPRL amplitude with the coherent-intertwiner boundary state. There are 2 critical points (of opposite 4-simplex orientations) with the fixed boundary state. Applying the asymptotic expansion (Hörmander's theorem 7.7.5 in [19]), we perform large- j asymptotic expansions the 4-simplex amplitude at both critical points, and compute numerically both the leading and next-to-leading contributions. If we scale spins by $j_f \rightarrow \lambda j_f$ for all boundary triangles f , the expansion in λ is represented as below

$$A_v^{(\pm)} = C^{(\pm)}(\gamma) \cdot \left[1 + \frac{\kappa^{(\pm)}(\gamma)}{\lambda} + O\left(\frac{1}{\lambda^2}\right) \right] \quad (1.1)$$

where $C^{(\pm)}$, $\kappa^{(\pm)}$ depending on the value of γ are computed numerically in this work. $C^{(\pm)}$ coincides with the leading order asymptotics by Barrett et al [8]. The next-to-leading order coefficient $\kappa^{(\pm)}(\gamma)$ is one of main interests in this work. It turns out that $\kappa^{(+)}(\gamma) = \overline{\kappa^{(-)}(\gamma)}$, and as a typical example, at $\gamma = 0.1$, $|\kappa^{(\pm)}(0.1)| \simeq 3.14$ and the 4-simplex amplitude $A_v = A_v^{(+)} + A_v^{(-)}$ is given by¹

$$A_v = \left(1 + \frac{1}{4\lambda}\right)^6 \left(1 + \frac{1}{10\lambda}\right)^4 \frac{3.55 \times 10^{-13}}{\lambda^{12}} e^{4.59\lambda i} \left[\cos(0.106 + 0.01\lambda) + \frac{3.14}{\lambda} \sin(-1.27 + 0.01\lambda) + O\left(\frac{1}{\lambda^2}\right) \right], \quad (1.2)$$

where $S_{Regge} = 0.01\lambda$ in the cosine and sine is the Regge action of the geometrical 4-simplex. The next-to-leading order has to be sufficiently small in order to validate the semiclassical approximation of A_v with the leading order as in [8]. By the above result, for example when $\lambda = 30$, $|\kappa^{(\pm)}(0.1)/\lambda| \simeq 0.1$ is about 10% of the leading order. Namely, approximating the amplitude $A_v^{(\pm)}$ by the leading order term $C^{(\pm)}(\gamma)$ at $\lambda = 30$ leads to the error at about 10% of the magnitude.

This conclusion becomes different when the boundary state is the coherent spin-network. With the same 4-simplex geometry and boundary data, the EPRL amplitude A'_v with the boundary coherent spin-network contains summing over j . The boundary coherent spin-network determines one critical point of the amplitude while eliminating the other. The asymptotic expansion gives

$$A'_v = C'(\gamma) \cdot \left[1 + \frac{\kappa'(\gamma)}{\lambda} + O\left(\frac{1}{\lambda^2}\right) \right]. \quad (1.3)$$

At $\gamma = 0.1$, the next-to-leading order coefficient gives $|\kappa'(0.1)| \simeq 40.67$. When $\lambda = 30$, $|\kappa'(0.1)/\lambda| \simeq 1.36$ is even greater than the leading order. Clearly the semiclassical approximation of A'_v is invalid at $\lambda = 30$, and a much greater λ is needed. For instance, when $\lambda \geq 300$, $|\kappa'(0.1)/\lambda|$ is bounded by about 13% of the leading order. We suggest the much safer zone to be $\lambda \geq 3000$ for A'_v ($\lambda \geq 300$ for A_v) where the next-to-leading order is about 1% of the leading order.

The increase of allowed λ in A'_v may due to the increase of degrees of freedom (DOFs) by including the sum over j in A'_v . Therefore we expect that an even larger λ may be required to validate the large- j expansion for general spinfoam amplitudes on many 4-simplices with summing over internal spins.

Moreover, we study numerically dependences of $\kappa^{(\pm)}$ and κ' on γ . Numerical results indicate that they stabilize to real constants asymptotically as $\gamma \rightarrow \infty$.

¹The next-to-leading order gives a sine function similar to the expansion of 6j symbol [20].

Main computations in this work are carried out with Mathematica. Mathematica codes for constructing critical points and computing large- j expansion can be found in [21]. Although our computation fixes the 4-simplex boundary data, the codes can easily adapt to other boundary data.

In addition, A_v in Eq.(1.2) can be rewritten as

$$A_v \simeq \left(1 + \frac{1}{4\lambda}\right)^6 \left(1 + \frac{1}{10\lambda}\right)^4 \frac{3.55 \times 10^{-13}}{\lambda^{12}} e^{4.59\lambda i} \left(1 - \frac{3.082}{\lambda} + O\left(\frac{1}{\lambda^2}\right)\right) \left[\cos\left(0.01\lambda + 0.106 - \frac{0.601}{\lambda} + O\left(\frac{1}{\lambda^2}\right)\right)\right]. \quad (1.4)$$

where the quantity inside the cosine:

$$S_{eff} = 0.01\lambda + 0.106 - \frac{0.601}{\lambda} + O\left(\frac{1}{\lambda^2}\right) \quad (1.5)$$

can be viewed as an ‘‘effective action’’ with quantum corrections to the Regge action $S_{Regge} = 0.01\lambda$.

Here are some other works on numerical analysis of spinfoam models from different perspectives: [18, 22] numerically compute the EPRL amplitude in the spin-intertwiner representation, by decomposing Clebsch-Gordan coefficients of $SL(2, \mathbb{C})$ in terms of those of $SU(2)$. [23, 24] numerically compute symmetry-restricted spinfoam models and their renormalizations.

This paper is organized as follows: Section 2 is a brief review of the EPRL 4-simplex amplitude. Section 3 explains the boundary data and the construction of critical points. New results of this paper start from Section 4, where we expand the amplitude with the coherent intertwiner boundary state and numerically compute both leading and next-to-leading order contributions for various values of γ . Section 5, we study the EPRL amplitude with the boundary coherent spin-network, and numerically compute both leading and next-to-leading orders for various values of γ .

2 EPRL 4-simplex amplitude

Here we focus on Lorentzian 4-dimensional spinfoam 4-simplex amplitude, illustrated by FIG.1, where each black box is dual to a boundary tetrahedron and each edge is dual to a triangle. Boundary tetrahedra are labelled by indices $a, b = 1, \dots, 5$ and carry group variables $g_a \in SL(2, \mathbb{C})$. The triangle dual to the edge is shared by the a -th and b -th tetrahedra and carries an $SU(2)$ spin j_{ab} . We firstly impose the boundary state made by a tensor product of 5 coherent intertwiners, one for each tetrahedron,

$$|i_a(\vec{j}, \vec{\xi})\rangle = \int_{SU(2)} dh_a \bigotimes_{b \neq a} h_a |j_{ab}, \xi_{ab}\rangle, \quad a = 1, \dots, 5, \quad (2.1)$$

where $|j_{ab}, \xi_{ab}\rangle$ is the $SU(2)$ coherent state. The EPRL 4-simplex amplitude with the boundary state has the integral expression [8–10, 25–27] which is particularly useful for studying the large- j asymptotic behavior.

$$A_v(j_{ab}, i_a) = \int \prod_{a=2}^5 dg_a \int_{(\mathbb{CP}^1)^{10}} e^S \prod_{a < b} \frac{d_{j_{ab}}}{\pi} \Omega_{ab}, \quad (2.2)$$

with $d_{j_{ab}} = 2j_{ab} + 1$. $g_a \in SL(2, \mathbb{C})$ associates to each tetrahedron. We gauge fix the first tetrahedron to $g_1 = \mathbb{1}$. dg_a is the Haar measure on $SL(2, \mathbb{C})$. Ω_{ab} is the measure on \mathbb{CP}^1 :

$$\Omega_{ab} = \frac{\Omega}{\langle Z_{ab}, Z_{ab} \rangle \langle Z_{ba}, Z_{ba} \rangle}, \quad (2.3)$$

where $|Z_{ab}\rangle = g_a^\dagger |z_{ab}\rangle$, $|Z_{ba}\rangle = g_b^\dagger |z_{ab}\rangle$ and $|z_{ab}\rangle$ is a 2-component spinor for each triangle ab . The Hermitian inner product is $\langle z, w \rangle = \bar{z}_0 w_0 + \bar{z}_1 w_1$. Here $\Omega = \frac{i}{2} (z_0 dz_1 - z_1 dz_0) \wedge (\bar{z}_0 d\bar{z}_1 - \bar{z}_1 d\bar{z}_0)$ is

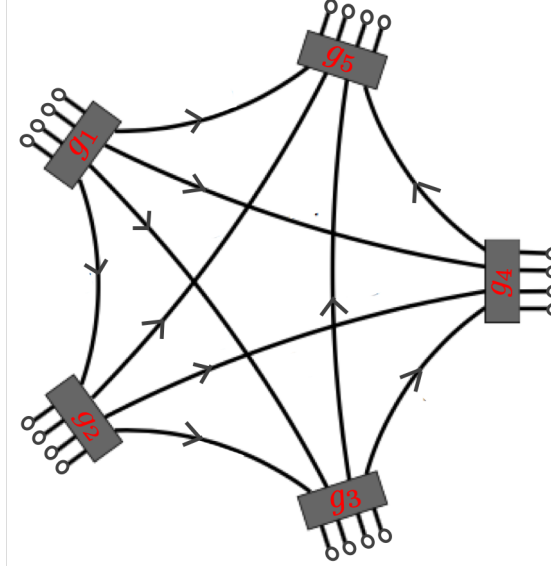


Figure 1. The graphical illustration of the 4-simplex amplitude: Five black boxes correspond to boundary tetrahedra carrying $g_a \in \text{SL}(2, \mathbb{C})$ ($a = 1, 2, 3, 4, 5$). Edges correspond to triangles carrying spins j_{ab} . Circles as endpoints of edges carry boundary states ξ_{ab} and ξ_{ba} . Arrows represent orientations $a < b$.

a homogeneous measure on \mathbb{C}^2 , and we choose the section of $\mathbb{C}\mathbb{P}^1$: $(z_0, z_1) \rightarrow (-\sin \frac{\Theta}{2} e^{-i\Phi}, \cos \frac{\Phi}{2})$, for which Ω reduces to $\Omega = \frac{\sin \Theta}{4} d\Phi d\Theta$.

The integrand in Eq.(2.2) is written as an exponential e^S with the action

$$S = \sum_{a < b} 2j_{ab} \ln \frac{\langle Z_{ab}, \xi_{ab} \rangle \langle J\xi_{ba}, Z_{ba} \rangle}{\langle Z_{ab}, Z_{ab} \rangle^{\frac{1}{2}} \langle Z_{ba}, Z_{ba} \rangle^{\frac{1}{2}}} + i\gamma j_{ab} \ln \frac{\langle Z_{ba}, Z_{ba} \rangle}{\langle Z_{ab}, Z_{ab} \rangle}, \quad (2.4)$$

where γ is the Barbero-Immirzi parameter and J is the anti-linear map

$$J \begin{pmatrix} z_0 \\ z_1 \end{pmatrix} = \begin{pmatrix} -\bar{z}_1 \\ \bar{z}_0 \end{pmatrix}.$$

The coherent state is labelled by the spin j_{ab} and a normalized 2-component spinor $|\xi_{ab}\rangle$ which is determined by $\hat{n}_{ab} = \langle \xi_{ab}, \vec{\sigma}\xi_{ab} \rangle$ ($\vec{\sigma}$ are Pauli matrices) the unit 3-normal \hat{n}_{ab} of the triangle ab in the boundary tetrahedron a .

To study the large- j behavior of the amplitude, we scale spins $j_{ab} \rightarrow \lambda j_{ab}$ by a large parameter λ . As a consequence of the scaling of spins, the action $S \mapsto \lambda S$. This scaling motivates us to study the asymptotical behavior of A_v in the large- j regime with the generalized stationary phase approximation analysis guided by Hörmander's theorem 7.7.5 in [19].

Theorem 2.1. *Let K be a compact subset in \mathbb{R}^n , X an open neighborhood of K , and k a positive integer. If (1) the complex functions $u \in C_0^{2k}(K)$, $f \in C^{3k+1}(X)$ and $\text{Im} f \geq 0$ in X ; (2) there is a unique point $x_0 \in K$ satisfying $\text{Im}(S(x_0)) = 0$, $f'(x_0) = 0$, and $\det(f''(x_0)) \neq 0$ (f'' denotes the Hessian matrix), $f' \neq 0$ in $K \setminus \{x_0\}$ then we have the following estimation:*

$$\left| \int_K u(x) e^{i\lambda f(x)} dx - e^{i\lambda f(x_0)} \left[\det \left(\frac{\lambda f''(x_0)}{2\pi i} \right) \right]^{-\frac{1}{2}} \sum_{s=0}^{k-1} \left(\frac{1}{\lambda} \right)^s L_s u(x_0) \right| \leq C \left(\frac{1}{\lambda} \right)^k \sum_{|\alpha| \leq 2k} \sup |D^\alpha u|. \quad (2.5)$$

Here the constant C is bounded when f stays in a bounded set in $C^{3k+1}(X)$. We have used the standard multi-index notation $\alpha = \langle \alpha_1, \dots, \alpha_n \rangle$ and

$$D^\alpha = (-i)^\alpha \frac{\partial^{|\alpha|}}{\partial x_1^{\alpha_1} \dots \partial x_n^{\alpha_n}}, \quad \text{where } |\alpha| = \sum_{i=1}^n \alpha_i \quad (2.6)$$

$L_s u(x_0)$ denotes the following operation on u :

$$L_s u(x_0) = i^{-s} \sum_{l-m=s} \sum_{2l \geq 3m} \frac{(-1)^l 2^{-l}}{l! m!} \left[\sum_{a,b=1}^n H_{ab}^{-1}(x_0) \frac{\partial^2}{\partial x_a \partial x_b} \right]^l (g_{x_0}^m u)(x_0), \quad (2.7)$$

where $H(x) = f''(x)$ denotes the Hessian matrix and the function $g_{x_0}(x)$ is given by

$$g_{x_0}(x) = f(x) - f(x_0) - \frac{1}{2} H^{ab}(x_0) (x - x_0)_a (x - x_0)_b$$

such that $g_{x_0}(x_0) = g'_{x_0}(x_0) = g''_{x_0}(x_0) = 0$. For each s , L_s is a differential operator of order $2s$ acting on $u(x)$.

Employing this Theorem, we can compute the 4-simplex amplitude in Eq.(2.2) as an $1/\lambda$ asymptotics series at critical points. As a consequence, the asymptotics of 4-simplex amplitude as $\lambda \rightarrow \infty$ is dominated by contributions of critical points which are the solutions of the critical point equations,

$$\text{Re}(S) = 0, \quad \partial_{z_{ab}} S = 0, \quad \text{and } \partial_{g_a} S = 0, \quad (2.8)$$

where $S[g, z]$ is given by Eq.(2.4). Results from literatures e.g. [8, 9, 26–28] show that for boundary states whose data j_{ab}, ξ_{ab} correspond to the geometrical boundary of a nondegenerate 4-simplex (and satisfy the orientation matching condition), S has 2 critical points having the geometrical interpretation as the nondegenerate geometrical 4-simplex with opposite orientations. S evaluated at critical points gives the Regge action of the 4-simplex with opposite sign. In the next section, we review the boundary data and the construction of critical points for the EPRL amplitude with the coherent-intertwiner boundary state.

3 Boundary data and critical point

3.1 Boundary data

The boundary state $|\psi\rangle = \otimes_{a=1}^5 |i_a\rangle$ for demonstrating our algorithm is the same as in [18]. $|\psi\rangle$ is labelled by 10 spin variables $\lambda_{j_{ab}}$ and 20 ξ_{ab} which relate to face 3-normals \vec{n}_{ab} . We set the area of 6 faces of the geometrical 4-simplex to be 2 and other 4 face areas to be 5. Although we use dimensionless numbers to describe the areas, physical areas are obtained by attaching proper units to those numbers. In our calculation, those areas are j_{ab} (spins are $\lambda_{j_{ab}}$). Furthermore, the face normals, denoted as \vec{n}_{ab} , are gained by the 4-simplex geometry. For convenience, we denote the five vertices of the 4-simplex as P_a and five tetrahedra as T_a , where $a \in \{1, 2, 3, 4, 5\}$. We firstly write down the coordinates of the vertices P_a in the Minkowski spacetime. Our starting point is the tetrahedra T_1 , which is an equilateral tetrahedron with all areas equaling to 5. We endow the vertices of T_1 with coordinates $P_1 = (0, 0, 0, 0)$, $P_2 = (0, 0, 0, -2\sqrt{5}/3^{1/4})$, $P_3 = (0, 0, -3^{1/4}\sqrt{5}, -3^{1/4}\sqrt{5})$ and $P_4 = (0, -2\sqrt{10}/3^{3/4}, -\sqrt{5}/3^{3/4}, -\sqrt{5}/3^{1/4})$ respectively. It means that we locally set up a frame (t, x, y, z) so that T_1 is embedded in the subspace expanded by x, y, z axis. The 4-simplex can be well located in our frame if one can find a coordinate of the vertex $P_5 = (t_1, x_1, y_1, z_1)$ such that the 4-d distance between P_5 and P_a ($a \neq 5$) are the same and areas of the triangles connecting P_5 to other P_a are all 2. By solving the system of equations, one can find P_5 is

$(-3^{-1/4}10^{-1/2}, -\sqrt{5/2}/3^{3/4}, -\sqrt{5}/3^{3/4}, -\sqrt{5}/3^{1/4})$. Then, from the coordinates of P_a , we calculate the 4-d normals N_a of each tetrahedra T_a respectively: From the vertices we compute the edge vectors l_{ae}^I of the tetrahedron a at edge e , with $I = 0, 1, 2, 3$ a Cartesian coordinate index. Then one can determine the 4-d normals, N_a , from the triple product of wedges with a common vertex determined by three edges labelled by $e = 1, 2, 3$ respectively

$$N_{aI} = \frac{\epsilon_{IJKL} l_{a1}^J l_{a2}^K l_{a3}^L}{\|\epsilon_{IJKL} l_{a1}^J l_{a2}^K l_{a3}^L\|},$$

where the norms and scalar products are given by the Minkowski metric $\eta = \text{diag}(-, +, +, +)$, and the epsilon symbol is of the convention $\epsilon_{0123} = 1$. Hence, 4-d normal vectors for each tetrahedron are given by:

$$\begin{aligned} N_1 &= (-1, 0, 0, 0), \quad N_2 = \left(\frac{5}{\sqrt{22}}, \sqrt{\frac{3}{22}}, 0, 0\right), \quad N_3 = \left(\frac{5}{\sqrt{22}}, -\frac{1}{\sqrt{66}}, \frac{2}{\sqrt{33}}, 0\right), \\ N_4 &= \left(\frac{5}{\sqrt{22}}, -\frac{1}{\sqrt{66}}, -\frac{1}{\sqrt{33}}, \frac{1}{\sqrt{11}}\right), \quad N_5 = \left(\frac{5}{\sqrt{22}}, -\frac{1}{\sqrt{66}}, -\frac{1}{\sqrt{33}}, -\frac{1}{\sqrt{11}}\right). \end{aligned} \quad (3.1)$$

The next step is to find the transformation which takes all 4-d normal vectors of tetrahedra to the time gauge $T = (-1, 0, 0, 0)$ [18]:

$$\begin{aligned} \Lambda_{aJ}^I &= \eta_J^I + \frac{1}{1 - N_a \cdot T} (N_a^I N_{aJ} + T^I T_J + N_a^I T_J - (1 - 2N_a \cdot T) T^I N_{aJ}), \\ \Lambda_{aJ}^I N_a^J &= T^I \quad \det \Lambda_{aJ}^I = 1, \quad a \neq 1, \quad I, J = 0, 1, 2, 3. \end{aligned}$$

Then 3-d face normals are

$$n_{ab}^I := -\Lambda_{aJ}^I \frac{N_b^J + N_a^J (N_a \cdot N_b)}{\sqrt{(N_a \cdot N_b)^2 - 1}}. \quad (3.2)$$

The gauge-fixed tetrahedron, $a = 1$, has $\Lambda_1 = \eta$ and $N_1 = T$. 3d normals resulting from Eq.(3.2) are showing in Table 1.

Table 1. Each cell of the table is the 3d normal vector coordinates for the face shared by line number tetrahedra and column number tetrahedra.

normal \vec{n}_{ab} \ b	1	2	3	4	5
a \ 1	\	(1,0,0)	(-0.33,0.94,0)	(-0.33,-0.47,0.82)	(-0.33,-0.47,-0.82)
2	(-1,0,0)	\	(0.83,0.55,0)	(0.83,-0.28,0.48)	(0.83,-0.28,-0.48)
3	(0.33,-0.94,0)	(0.24,0.97,0)	\	(-0.54,0.69,0.48)	(-0.54,0.69,-0.48)
4	(0.33,0.47,-0.82)	(0.24,-0.48,0.84)	(-0.54,0.068,0.84)	\	(-0.54,-0.76,0.36)
5	(0.33,0.47,0.82)	(0.24,-0.48,-0.84)	(-0.54,0.068,-0.84)	(-0.54,-0.76,-0.36)	\

\vec{n}_{ab} can be converted to the spinor $|\xi_{ab}\rangle$ (by fixing the phase convention):

$$\vec{n}_{ab} = (\sin \Theta \cos \Phi, \sin \Theta \sin \Phi, \cos \Theta) \rightarrow |\xi_{ab}\rangle = \left(-\sin \frac{\Theta}{2} e^{-i\Phi}, \cos \frac{\Phi}{2}\right). \quad (3.3)$$

Resulting $|\xi_{ab}\rangle$ for the boundary state is showing in Table 2. Once boundary data j_{ab}, ξ_{ab} are fixed, critical points (g_a^0, z_{ab}^0) are obtained by solving critical point equations (2.8).

Table 2. Each cell of the table is boundary state coordinates for the face shared by line number tetrahedra and column number tetrahedra.

$ \xi_{ab}\rangle$ a \ b	1	2	3	4	5
1	\	(0.71,0.71)	(0.71,-0.24+0.67 i)	(0.95,-0.17-0.25 i)	(0.30,-0.55-0.78 i)
2	(0.71,-0.71)	\	(0.71,0.59+0.39 i)	(0.86, 0.48 - 0.16 i)	(0.51, 0.82 - 0.27 i)
3	(0.71, 0.24 - 0.67 i)	(0.71, 0.17 + 0.69 i)	\	(0.86, -0.31 + 0.40 i)	(0.51, -0.53 + 0.68 i)
4	(0.30, 0.55 + 0.78 i)	(0.96, 0.13 - 0.25 i)	(0.96, -0.28 + 0.035 i)	\	(0.83, -0.33 - 0.46 i)
5	(0.95, 0.17 + 0.25 i)	(0.28, 0.43 - 0.86 i)	(0.28, -0.95 + 0.12 i)	(0.57, -0.48-0.67 i)	\

3.2 Critical points

Critical points of the integral (2.2) are denoted by (g_a^0, z_{ab}^0) . From the critical point equations (2.8), $\text{Re}(S) = 0$ leads to the equations [26]

$$|\xi_{ab}\rangle = \frac{e^{i\psi_{ab}}}{\|Z_{ab}\|} g_a^\dagger |z_{ab}\rangle, \quad \text{and} \quad |J\xi_{ba}\rangle = \frac{e^{i\psi_{ba}}}{\|Z_{ba}\|} g_a^\dagger |z_{ab}\rangle, \quad (3.4)$$

where $\|Z_{ab}\| \equiv |\langle Z_{ab}, Z_{ab} \rangle|^{1/2}$, ψ_{ab} and ψ_{ba} are phases. The two equations above can be combined to

$$(g_a^\dagger)^{-1} |\xi_{ab}\rangle = \frac{\|Z_{ba}\|}{\|Z_{ab}\|} e^{i(\psi_{ab}-\psi_{ba})} (g_b^\dagger)^{-1} |J\xi_{ba}\rangle. \quad (3.5)$$

The variation of the action with respect to a spinor $\partial_{z_{ab}} S = 0$ leads to the equation

$$g_a |\xi_{ab}\rangle = \frac{\|Z_{ab}\|}{\|Z_{ba}\|} e^{i(\psi_{ab}-\psi_{ba})} g_b |J\xi_{ba}\rangle. \quad (3.6)$$

The variation with respect to g_a gives the closure condition

$$\sum_b j_{ab} \vec{n}_{ab} = 0. \quad (3.7)$$

Solutions of above equations have been studied extensively in the literature. Given the boundary data j_{ab}, ξ_{ab} which satisfies the orientation matching condition, then above equations have 2 solutions corresponding to the 4-simplex geometry with opposite orientations [8]. These solutions are denoted by $(g^{0(\pm)}, z^{0(\pm)})$. $g^{0(\pm)}$ relates to the Lorentz transformation acting on each tetrahedron T_a and gluing them together to form the 4-simplex. They can be expressed explicitly [18] by $g_1^0 = \mathbb{1}$

$$g_a^{0(\pm)} = \exp \left((\pm \theta_{1a}^L + i\pi) \vec{n}_{1a} \cdot \frac{\vec{\sigma}}{2} \right), \quad a \neq 1, \quad (3.8)$$

where $\vec{\sigma}$ are Pauli matrices. θ_{1a}^L is the 4-d dihedral angle which is the boost angle between two 4-d normals of tetrahedra, defined by:

$$N_1 \cdot N_a = \cosh \theta_{1a}^L, \quad a \neq 1, \quad (3.9)$$

where N_1 and N_a are given by (3.1). From Eq. (3.8), we can see that $g_a^{0(\pm)}$ are combinations of boosts given by $\pm \theta_{1a}^L$ and an additional rotation π in the same direction. Resulting from this rotation, 3-d normals in the first tetrahedron are opposite to the corresponding ones in the adjacent tetrahedra. The numerical results for critical point $g_a^{0(\pm)}$ are shown in Table 3.

z_{ab} can be fixed by $g_a^{0(\pm)}$ and $|\xi_{ab}\rangle$, up to a complex scaling, by the first equation in Eqs.(3.4)

$$|z_{ab}^{0(\pm)}\rangle \propto_{\mathbb{C}} (g_a^{0(\pm)\dagger})^{-1} |\xi_{ab}\rangle. \quad (3.10)$$

Table 3. Each cell of the table is the critical point of a-th tetrahedron group element $g_a^{0(\pm)}$.

a	1	2	3	4	5
$g_a^{0(+)}$	$\begin{pmatrix} 1 & 0 \\ 0 & 1 \end{pmatrix}$	$\begin{pmatrix} 0.18i & 1.01i \\ 1.01i & 0.18i \end{pmatrix}$	$\begin{pmatrix} 0.18i & 0.96 - 0.34i \\ -0.96 - 0.34i & 0.18i \end{pmatrix}$	$\begin{pmatrix} 1.01i & -0.48 - 0.34i \\ 0.48 - 0.34i & -0.65i \end{pmatrix}$	$\begin{pmatrix} -0.65i & -0.48 - 0.34i \\ 0.48 - 0.34i & 1.01i \end{pmatrix}$
$g_a^{0(-)}$	$\begin{pmatrix} 1 & 0 \\ 0 & 1 \end{pmatrix}$	$\begin{pmatrix} -0.18i & -1.01i \\ 1.01i & -0.18i \end{pmatrix}$	$\begin{pmatrix} -0.18i & 0.96 - 0.34i \\ -0.96 - 0.34i & -0.18i \end{pmatrix}$	$\begin{pmatrix} 0.65i & -0.48 - 0.34i \\ 0.48 - 0.34i & -1.01i \end{pmatrix}$	$\begin{pmatrix} -1.01i & -0.48 - 0.34i \\ 0.48 - 0.34i & 0.65i \end{pmatrix}$

Scaling of z_{ab} is a gauge transformation of S . We fix the scaling by normalizing $|z_{ab}^{0(\pm)}\rangle$ and making the following parametrization

$$|z_{ab}^{0(\pm)}\rangle = \begin{pmatrix} -\sin \frac{\theta_{ab}^{0(\pm)}}{2} e^{-i\phi_{ab}^{0(\pm)}} \\ \cos \frac{\theta_{ab}^{0(\pm)}}{2} \end{pmatrix}, \quad (3.11)$$

here, $\theta_{ab}^{0(\pm)}$ and $\phi_{ab}^{0(\pm)}$ are real.

The numerical results for $(\theta_{ab}^{0(\pm)}, \phi_{ab}^{0(\pm)})$ are shown in Table 4. All critical point data of $z_{ab}^{0(\pm)}$ and $g_a^{0(\pm)}$ can be found in Mathematica notebooks in [21], which contain codes demonstrating that the data satisfy the critical point equations (2.8) with the boundary data.

Table 4. Each cell of the table is critical point parameterized by $(\theta_{ab}^{0(\pm)}, \phi_{ab}^{0(\pm)})$ for the face shared by line number tetrahedron a and column number tetrahedron b, $a < b$. Two tables list the result for two distinct critical points.

$(\theta_{ab}^{0(+)}, \phi_{ab}^{0(+)})$ \ a \ b	2	3	4	5
1	(-1.57,0)	(-1.57,1.91)	(-2.53,-2.19)	(-0.62,-2.19)
2	\	(-1.57,-0.82)	(-0.89, 0.49)	(-2.25, 0.49)
3	\	\	(-0.89, 1.42)	(-2.25, 1.42)
4	\	\	\	(-2.94, 0.96)

$(\theta_{ab}^{0(-)}, \phi_{ab}^{0(-)})$ \ a \ b	2	3	4	5
1	(-1.57,0)	(-1.57,1.91)	(-2.53,-2.19)	(-0.62,-2.19)
2	\	(-1.57,-0.41)	(-1.21, 0.22)	(-1.93, 0.22)
3	\	\	(-1.21, 1.69)	(-1.93, 1.69)
4	\	\	\	(-2.94, -2.19)

It is possible to add other boundary geometries to the analysis. Here, we adapt this boundary geometry in order to consist with the results in [18].

4 Next-to-leading order correction in large- j 4-simplex amplitude with coherent-intertwiner boundary state

4.1 Explicit expression of 4-simplex amplitude

Given one of the critical points of the 4-simplex amplitude, we make following parametrizations of g_a and z_{ab} of the neighborhood of the critical point in the integration domain of Eq.(2.2): The group variable $g_a \in \text{SL}(2, \mathbb{C})$ is parametrized by

$$g_a(x_{a1}, y_{a1}, x_{a2}, y_{a2}, x_{a3}, y_{a3}) = g_a^{0(\pm)} \begin{pmatrix} 1 + \frac{x_{a1} + iy_{a1}}{\sqrt{2}} & \frac{x_{a2} + iy_{a2}}{\sqrt{2}} \\ \frac{x_{a3} + iy_{a3}}{\sqrt{2}} & 1 + \frac{x_{a2} + iy_{a2}}{\sqrt{2}} \frac{x_{a3} + iy_{a3}}{\sqrt{2}} \\ & 1 + \frac{x_{a1} + iy_{a1}}{\sqrt{2}} \end{pmatrix}, \quad (4.1)$$

where x_{ai} and y_{ai} ($a \neq 1, i = 1, 2, 3$) are real. The first tetrahedron is gauge-fixed, $g_1 = \mathbb{1}$. One need 24 real variables x_{ai} and y_{ai} ($a = 2, 3, 4, 5$) to parametrize all g_a . The spinor $z_{ab} \in \mathbb{CP}^1$ is

parametrized by

$$z_{ab}(\Theta_{ab}, \Phi_{ab}) = \begin{pmatrix} -\sin\left(\frac{\theta_{ab}^{0(\pm)} + \Theta_{ab}}{2}\right) e^{-i(\phi_{ab}^{0(\pm)} + \Phi_{ab})} \\ \cos\left(\frac{\theta_{ab}^{0(\pm)} + \Theta_{ab}}{2}\right) \end{pmatrix}. \quad (4.2)$$

Each triangle ab has 2 real variables Θ_{ab} and Φ_{ab} , so we need in total 20 real variables to describe z_{ab} . $|Z_{ab}\rangle = g_a^\dagger z_{ab}$ follows from (4.1) and (4.2). The arguments of the action in Eq.(2.4) are now x_{ai} , y_{ai} , Θ_{ab} and Φ_{ab} .

For the group integral, the $\text{SL}(2, \mathbb{C})$ Haar measure dg can be written explicitly by

$$\prod_{a=2}^5 dg_a = \prod_{a=2}^5 \frac{1}{2^7 \pi^4} \frac{dx_{a1} dy_{a1} dx_{a2} dy_{a2} dx_{a3} dy_{a3}}{\left|1 + \frac{x_{a1} + iy_{a1}}{\sqrt{2}}\right|^2}. \quad (4.3)$$

The details of this derivation are in appendix A. We define the function $u(x_{ai}, y_{ai}, \Theta_{ab}, \Phi_{ab})$ by

$$u(x_{ai}, y_{ai}, \Theta_{ab}, \Phi_{ab}) \prod_{a < b} \prod_{i=1,2,3} dx_{ai} dy_{ai} d\Phi_{ab} d\Theta_{ab} = \prod_{a < b} \Omega_{ab} dg_a, \quad (4.4)$$

where Ω_{ab} is the measure on \mathbb{CP}^1 in (2.3):

$$\Omega_{ab} = \frac{\sin\left(\theta_{ab}^{0(\pm)} + \Theta_{ab}\right)}{4\langle Z_{ab}, Z_{ab} \rangle \langle Z_{ba}, Z_{ba} \rangle} d\Theta_{ab} d\Phi_{ab}. \quad (4.5)$$

There are 44 arguments in $u(x_{ai}, y_{ai}, \Theta_{ab}, \Phi_{ab})$. The amplitude (2.2) gives

$$\prod_{a < b} \frac{d\lambda_{jab}}{\pi} \int \prod_{i=1}^{44} dx_i u(\vec{x}) e^{\lambda S(\vec{x})}, \quad (4.6)$$

where $\vec{x} = (x_1, x_2, \dots, x_{44}) \equiv (x_{ai}, y_{ai}, \Theta_{ab}, \Phi_{ab})$ contains 44 components. Eq.(4.6) expresses the EPRL 4-simplex amplitude in the form as Eq.(2.7). Besides, the critical point for $S(\vec{x})$ is at $\vec{x}_0 = (0, 0, \dots, 0)$. Next, we will apply Theorem 2.1 to expand the integral (4.6) and numerically compute the leading and next-to-leading order contributions.

We emphasize that the parametrization \vec{x} is within the neighborhood of *one* critical point in the integration domain, and (4.6) is A_v restricted in the neighborhood. A_v has 2 critical points which leads to 2 different notions of \vec{x} . We don't put the label e.g. (\pm) to \vec{x} in order to make notations less cumbersome.

4.2 Asymptotic expansion and next-to-leading order correction

Following the convention in Theorem 2.1, we rewrite the exponent in the integrand

$$\int \prod_{i=1}^{44} dx_i u(\vec{x}) e^{\lambda S(\vec{x})} = \int \prod_{i=1}^{44} dx_i u(\vec{x}) e^{i\lambda \tilde{S}(\vec{x})}.$$

Here, $\tilde{S}(\vec{x}) = -iS(\vec{x})$, Hessian matrix $H_{ij}(\vec{x}) = \partial_i \partial_j \tilde{S}(\vec{x})$. The leading and the next-to-leading order terms in Eq.(2.7) correspond to $s = 0$ and $s = 1$. In (2.7), the expression of $L_s u(x_0)$ sums a finite number of terms for each s .

Our scheme of computation is as follows: At $s = 0$, the corresponding term for $L_{s=0} u(\vec{x})$ is

$$I_0 = u(0). \quad (4.7)$$

At $s = 1$, the possible (m, l) are $(0, 1), (1, 2), (2, 3)$ to satisfy $2l \geq 3m$. The corresponding terms are of the types:

1) $(m, l) = (0, 1)$:

$$I_1 = -\frac{1}{2i} \left[\sum_{i,j=1}^{44} H_{ij}^{-1}(0) \frac{\partial^2 u(0)}{\partial x_i \partial x_j} \right]. \quad (4.8)$$

where we have express $\vec{x} = (x_1, x_2, \dots, x_{44})$. We compute the second-order derivative of the function $u(\vec{x})$ with respect to x_i and x_j and evaluate the result at $\vec{x} = 0$. We save the resulting 44×44 matrix $\frac{\partial^2 u(0)}{\partial x_i \partial x_j}$ and contract it with the Hessian matrix.

2) $(m, l) = (1, 2)$: We define

$$g_{x_0}(\vec{x}) = \tilde{S}(\vec{x}) - \tilde{S}(0) - \frac{1}{2} \sum_{i,j=1}^{44} H_{ij}(0) x_i x_j, \quad (4.9)$$

$$\begin{aligned} I_2 &= \frac{1}{8i} \left[\sum_{i,j=1}^{44} H_{ij}^{-1}(0) \frac{\partial^2}{\partial x_i \partial x_j} \right] \left[\sum_{k,l=1}^{44} H_{kl}^{-1}(0) \frac{\partial^2}{\partial x_k \partial x_l} \right] (g_{x_0} u)(0) \\ &= \frac{1}{8i} \left[\sum_{i,j,k,l=1}^{44} H_{ij}^{-1} H_{kl}^{-1} \frac{\partial^4}{\partial x_i \partial x_j \partial x_k \partial x_l} \right] (g_{x_0} u)(0) \\ &= \frac{1}{8i} \sum_{i,j,k,l=1}^{44} H_{ij}^{-1} H_{kl}^{-1} \left[\frac{\partial^3 g_{x_0}(0)}{\partial x_i \partial x_j \partial x_k} \frac{\partial u(0)}{\partial x_l} + \frac{\partial^3 g_{x_0}(0)}{\partial x_i \partial x_j \partial x_l} \frac{\partial u(0)}{\partial x_k} + \frac{\partial^3 g_{x_0}(0)}{\partial x_j \partial x_k \partial x_l} \frac{\partial u(0)}{\partial x_i} \right. \\ &\quad \left. + \frac{\partial^3 g_{x_0}(0)}{\partial x_i \partial x_k \partial x_l} \frac{\partial u(0)}{\partial x_j} + \frac{\partial^4 g_{x_0}(0)}{\partial x_i \partial x_j \partial x_k \partial x_l} u(0) \right]. \end{aligned} \quad (4.10)$$

To compute less expensively, we use following techniques in our code [21]. First, for $\partial^3 g_{x_0}(0)$ and $\partial^4 g_{x_0}(0)$, there are 44^3 possible third order partial derivatives and 44^4 fourth order partial derivatives. However, for function $g_{x_0}(\vec{x})$, the mixed partial derivatives are equal, which means that the order in which we differentiate won't matter. To save space, we save $\partial^3 g_{x_0}(0)$ as a 3-d upper "triangle" array $G^{(3)}$ and $\partial^4 g_{x_0}(0)$ as a 4-d upper "triangle" array $G^{(4)}$. Hence, the size of the array is deduced from 44^d to $\binom{44+d-1}{d}$. Secondly, because of the symmetric property of the Hessian matrix, we can simplify the above summation from $\sum_{i,j,k,l=1}^{44} F_{ijkl}$ to $\sum_{i=1}^{44} \sum_{j=1}^i \sum_{k=1}^j \sum_{l=1}^k \tilde{F}_{ijkl}$, here we use F_{ijkl} to denote the factors' product in Eq.(4.10). To be clear, we use an example $i = 9, j = 8, k = 8, l = 1$, i.e., $(9, 8, 8, 1)$, to explain the technique. We sum all possible $H_{ij}^{-1} H_{kl}^{-1}$ first, it's $4H_{19}^{-1} H_{88}^{-1} + 8H_{81}^{-1} H_{89}^{-1}$. Here, we use the symmetric property of H^{-1} and the counting principle to get each terms and the corresponding coefficient. In this case,

$$\begin{aligned} \tilde{F}_{9881} &= (4H_{19}^{-1} H_{88}^{-1} + 8H_{81}^{-1} H_{89}^{-1}) \\ &\quad \times \left(G_{988}^{(3)} \frac{\partial u(0)}{\partial x_1} + 2 \times G_{981}^{(3)} \frac{\partial u(0)}{\partial x_8} + G_{881}^{(3)} \frac{\partial u(0)}{\partial x_9} + G_{9881}^{(4)} u(0) \right). \end{aligned} \quad (4.11)$$

One can find the details in our Mathematica notebooks [21].

3) $(m, l) = (2, 3)$:

$$\begin{aligned}
I_3 &= -\frac{1}{96i} \left[\sum_{i,j,k,l,m,n=1}^{44} H_{ij}^{-1} H_{kl}^{-1} H_{mn}^{-1} \frac{\partial^6}{\partial x_i \partial x_j \partial x_k \partial x_l \partial x_m \partial x_n} \right] (g_{x_0}^2 u)(0) \\
&= -\frac{1}{48i} \sum_{i,j,k,l,m,n=1}^{44} H_{ij}^{-1} H_{kl}^{-1} H_{mn}^{-1} \left[\frac{\partial^3 g_{x_0}(0)}{\partial x_j \partial x_k \partial x_l} \frac{\partial^3 g_{x_0}(0)}{\partial x_i \partial x_m \partial x_n} \right. \\
&\quad + \frac{\partial^3 g_{x_0}(0)}{\partial x_j \partial x_k \partial x_m} \frac{\partial^3 g_{x_0}(0)}{\partial x_i \partial x_l \partial x_n} + \frac{\partial^3 g_{x_0}(0)}{\partial x_j \partial x_k \partial x_n} \frac{\partial^3 g_{x_0}(0)}{\partial x_i \partial x_l \partial x_m} \\
&\quad + \frac{\partial^3 g_{x_0}(0)}{\partial x_j \partial x_l \partial x_m} \frac{\partial^3 g_{x_0}(0)}{\partial x_i \partial x_k \partial x_n} + \frac{\partial^3 g_{x_0}(0)}{\partial x_j \partial x_l \partial x_n} \frac{\partial^3 g_{x_0}(0)}{\partial x_i \partial x_k \partial x_m} \\
&\quad + \frac{\partial^3 g_{x_0}(0)}{\partial x_j \partial x_m \partial x_n} \frac{\partial^3 g_{x_0}(0)}{\partial x_i \partial x_k \partial x_l} + \frac{\partial^3 g_{x_0}(0)}{\partial x_k \partial x_l \partial x_m} \frac{\partial^3 g_{x_0}(0)}{\partial x_i \partial x_j \partial x_n} \\
&\quad + \frac{\partial^3 g_{x_0}(0)}{\partial x_k \partial x_l \partial x_n} \frac{\partial^3 g_{x_0}(0)}{\partial x_i \partial x_j \partial x_m} + \frac{\partial^3 g_{x_0}(0)}{\partial x_k \partial x_m \partial x_n} \frac{\partial^3 g_{x_0}(0)}{\partial x_i \partial x_j \partial x_l} \\
&\quad \left. + \frac{\partial^3 g_{x_0}(0)}{\partial x_l \partial x_m \partial x_n} \frac{\partial^3 g_{x_0}(0)}{\partial x_i \partial x_j \partial x_k} \right] u(x_0). \tag{4.12}
\end{aligned}$$

We have deduced sixth-order derivative to third-order derivatives with the condition $g_{x_0}(0) = 0$, $g'_{x_0}(0) = 0$ and $g''_{x_0}(0) = 0$. Factors in each term in the square-bracket in (4.12) are elements which we have stored in table $G^{(3)}$. We use similiar techniques in 2) to simplify the summation in (4.12) to make the computation less expensive.

4.3 Numerical results

The asymptotic result for the integral (4.6) is:

$$\begin{aligned}
A_v &= A_v^{(+)} + A_v^{(-)}, \\
A_v^{(\pm)} &= A_v^{(\pm)0} + A_v^{(\pm)1} + O\left(\frac{1}{\lambda^2}\right), \\
A_v^{(\pm)0} &= 2^4 \prod_{a < b} \frac{d\lambda_{jab}}{\pi} e^{i\lambda\tilde{S}(\tilde{\mathbf{x}}_0^\pm)} \left[\det\left(\frac{\lambda S''(\tilde{\mathbf{x}}_0^\pm)}{2\pi i}\right) \right]^{-\frac{1}{2}} u(\tilde{\mathbf{x}}_0^\pm), \\
A_v^{(\pm)1} &= 2^4 \prod_{a < b} \frac{d\lambda_{jab}}{\pi} e^{i\lambda\tilde{S}(\tilde{\mathbf{x}}_0^\pm)} \left[\det\left(\frac{\lambda S''(\tilde{\mathbf{x}}_0^\pm)}{2\pi i}\right) \right]^{-\frac{1}{2}} \frac{1}{\lambda} (I_1 + I_2 + I_3)(\tilde{\mathbf{x}}_0^\pm). \tag{4.13}
\end{aligned}$$

where $A_v^{(+)}$ and $A_v^{(-)}$ are asymptotic expansions of A_v at two distinct critical points $\tilde{\mathbf{x}}_0^\pm$ corresponding to the geometrical 4-simplex with opposite orientation. $A_v^{(\pm)0}$ stands for the leading-order term of the asymptotics and $A_v^{(\pm)1}$ is the next-to-leading order correction. The additional factor 2^4 comes from the double multiplicity of the solutions $g_a = \pm g^0$ for $a \neq 1$. We evaluate the leading-order term and the next-to-leading order corrections at $\gamma = 0.1$ as an example:

$$\begin{aligned}
A_v^{(+)} &= \left(1 + \frac{1}{4\lambda}\right)^6 \left(1 + \frac{1}{10\lambda}\right)^4 \frac{1.77 \times 10^{-13} + 1.87 \times 10^{-14}i}{\lambda^{12}} e^{4.60\lambda i} \left(1 - \frac{3.082 + 0.601i}{\lambda}\right), \\
A_v^{(-)} &= \left(1 + \frac{1}{4\lambda}\right)^6 \left(1 + \frac{1}{10\lambda}\right)^4 \frac{1.77 \times 10^{-13} - 1.87 \times 10^{-14}i}{\lambda^{12}} e^{4.58\lambda i} \left(1 - \frac{3.082 - 0.601i}{\lambda}\right), \tag{4.14}
\end{aligned}$$

where 4.60 and 4.58 in exponents are corresponding values of $\tilde{S}(\vec{x}_0^\pm)$. The prefactor $(1 + \frac{1}{4\lambda})^6 (1 + \frac{1}{10\lambda})^4 = \prod_{a<b} d_{\lambda j_{ab}} / (2\lambda j_{ab})$ and

$$2^4 \prod_{a<b} \frac{2\lambda j_{ab}}{\pi} \left[\det \left(\frac{\lambda S''(\vec{x}_0^\pm)}{2\pi i} \right) \right]^{-\frac{1}{2}} u(\vec{x}_0^\pm) = \frac{1.77 \times 10^{-13} \pm 1.87 \times 10^{-14}i}{\lambda^{12}}. \quad (4.15)$$

We obtain the asymptotics of the EPRL 4-simplex amplitude A_v with the next-to-leading order correction as

$$A_v = \left(1 + \frac{1}{4\lambda}\right)^6 \left(1 + \frac{1}{10\lambda}\right)^4 \frac{3.55 \times 10^{-13}}{\lambda^{12}} e^{4.59\lambda i} \left[\cos(0.106 + 0.01\lambda) + \frac{3.14}{\lambda} \sin(-1.27 + 0.01\lambda) + O\left(\frac{1}{\lambda^2}\right) \right]. \quad (4.16)$$

It has been arranged in terms of cosines and sines, similar to the case of 6j symbol [20]. The Regge action S_{Regge} of the geometrical 4-simplex is inside the cosine and sine

$$S_{Regge} = \lambda \sum_{a<b} \gamma j_{ab} \theta_{ab}^L = 0.01\lambda. \quad (4.17)$$

Next, we combine cosines and sines in Eq.(4.16) to be in a nicer form. As $\lambda \rightarrow \infty$, we can expand $\log\left(1 - \frac{3.082 \pm 0.601i}{\lambda}\right)$ to 1st order in $1/\lambda$

$$1 - \frac{3.082 \pm 0.601i}{\lambda} \approx \exp\left(-\frac{3.082}{\lambda}\right) \exp\left(\pm \frac{0.601i}{\lambda}\right) \approx \left(1 - \frac{3.082}{\lambda}\right) \exp\left(\pm \frac{0.601i}{\lambda}\right). \quad (4.18)$$

Hence, (4.16) can be rewritten as

$$A_v \simeq \left(1 + \frac{1}{4\lambda}\right)^6 \left(1 + \frac{1}{10\lambda}\right)^4 \frac{3.55 \times 10^{-13}}{\lambda^{12}} e^{4.59\lambda i} \left(1 - \frac{3.082}{\lambda}\right) \left[\cos\left(0.01\lambda + 0.106 - \frac{0.601}{\lambda}\right) \right]. \quad (4.19)$$

where the quantity inside the cosine:

$$S_{eff} = 0.01\lambda + 0.106 - \frac{0.601}{\lambda} \quad (4.20)$$

can be viewed as an ‘‘effective action’’ with quantum corrections to the Regge action. Moreover, we can read the relative magnitude of leading-order and next-leading order correction by the factor $(1 - \frac{3.082}{\lambda})$ in Eq.(4.19).

Both the leading and next-to-leading order terms depend on γ , we write the asymptotic amplitude as

$$A_v^{(\pm)} \approx C^{(\pm)}(\gamma) \left(1 + \frac{\kappa^{(\pm)}(\gamma)}{\lambda}\right), \quad (4.21)$$

which reduces to (4.14) when $\gamma = 0.1$. Here, $C^{(\pm)}(\gamma)$ coincides with the leading order asymptotics. $\kappa^{(\pm)}(\gamma)$ is the next-to-leading order coefficient. $C^{(\pm)}(\gamma), \kappa^{(\pm)}$ depending on the value of γ . The ratio of next-to-leading order corrections to leading-order term is

$$\frac{\kappa^{(\pm)}(\gamma)}{\lambda} = \frac{1}{\lambda} \frac{I^{(\pm)}(\gamma)}{u(\vec{x}_0^\pm)}, \quad (4.22)$$

here, $u(\vec{\mathbf{x}}_0^+) = \frac{0.0073}{2^{48}\pi^{16}}$ and $u(\vec{\mathbf{x}}_0^-) = \frac{0.28}{2^{48}\pi^{16}}$ are independent on γ , $I^{(\pm)}(\gamma) = (I_1 + I_2 + I_3)(\vec{\mathbf{x}}_0^\pm)$ depends on γ , and

$$\kappa^{(+)}(\gamma) = \overline{\kappa^{(-)}(\gamma)}. \quad (4.23)$$

We use $|\kappa(\gamma)|$ to denote $|\kappa^{(+)}(\gamma)|$ and $|\kappa^{(-)}(\gamma)|$. We show some results of $|I^{(\pm)}(\gamma)|$ and $|\kappa(\gamma)|$ at different γ in Table 5. We plot $|\kappa(\gamma)|$ and $\kappa^{(+)}(\gamma)$ versus γ in Figure 2.

Table 5. $|I^{(\pm)}(\gamma)|$ and $|\kappa(\gamma)|$ with respect to γ .

γ		0.1	0.5	1	2	3	4	5	8
$2^{48}\pi^{16}$	$I^{(+)}(\gamma)$	0.023	0.033	0.044	0.047	0.042	0.037	0.033	0.025
$2^{48}\pi^{16}$	$I^{(-)}(\gamma)$	0.87	1.28	1.70	1.80	1.60	1.41	1.26	0.97
$ \kappa(\gamma) $		3.14	4.6	6.10	6.46	5.75	5.07	4.53	3.46
γ		10	20	50	100	200	500	800	1000
$2^{48}\pi^{16}$	$I^{(+)}(\gamma)$	0.022	0.013	0.007	0.006	0.0056	0.0055	0.0055	0.0055
$2^{48}\pi^{16}$	$I^{(-)}(\gamma)$	0.83	0.50	0.28	0.23	0.22	0.21	0.21	0.21
$ \kappa(\gamma) $		2.99	1.77	1.01	0.83	0.78	0.77	0.76	0.76

Table 5 and Figure 2 demonstrate how the next-to-leading order correction changes with different values of γ . $|\kappa(\gamma)|$ increases first and then decrease with increasing γ , and the maximum occurs at around $\gamma = 2$. Figure 2 (b) and (c) show that $\kappa^{(\pm)}(\gamma)$ stabilize to real constants 0.76 as $\gamma \rightarrow \infty$.

The semiclassical approximation of A_v with the leading order as in [8] is valid when λ is large enough so that $\frac{\kappa^{(\pm)}(\gamma)}{\lambda}$ is negligible comparing to 1. For example, at $\lambda = 30$ and $\gamma = 0.1$, $|\kappa(\gamma)|/\lambda \approx 0.10$ is about 10% of the leading order. In our opinion, a much safer regime for validating the semiclassical approximation needs an even larger λ , e.g. $\lambda = 300$ so that $|\kappa(\gamma)|/\lambda \approx 0.01$.

5 Next-to-leading order correction in large- j 4-simplex amplitude with coherent spin-network boundary state

5.1 Coherent spin network state

Above discussions take the coherent-intertwiners as the boundary state for the spinfoam amplitude. In this section, we use the coherent spin-network as the boundary state. The coherent spin-network relates to coherent intertwiners by a superposition

$$|\Psi_0\rangle = \sum_{j_{ab} \in \mathbb{Z}_+/2 \cup \{0\}} \psi_{j_0, \phi_0}(\vec{j}) \otimes_{a=1}^5 |i_a(\vec{j}, \vec{\xi})\rangle, \quad (5.1)$$

where $\psi_{j_0, \phi_0}(\vec{j})$ is given by,

$$\psi_{j_0, \phi_0}(\vec{j}) = \exp\left(-i \sum_{ab} \gamma \phi_0^{ab} (j_{ab} - (j_0)_{ab})\right) \exp\left(-\frac{1}{2} \sum_{ab, cd} \alpha^{(ab)(cd)} \frac{j_{ab} - (j_0)_{ab}}{\sqrt{(j_0)_{ab}}} \frac{j_{cd} - (j_0)_{cd}}{\sqrt{(j_0)_{cd}}}\right), \quad (5.2)$$

which is a gaussian times a phase. $(j_0)_{ab} \in \mathbb{Z}_+/2$. ϕ_0^{ab} is the discrete extrinsic curvature relating to the dihedral angle of the triangle ab in a 4-simplex geometry. Here we choose $(j_0)_{ab} = (2, 5)\lambda$ and ξ_{ab} are the same boundary data as above discussions. We set values of ϕ_0^{ab} by

$$\gamma \phi_0^{ab} = \frac{\partial \tilde{S}(\vec{j}, \vec{\mathbf{x}}_0^+)}{\partial j_{ab}}. \quad (5.3)$$

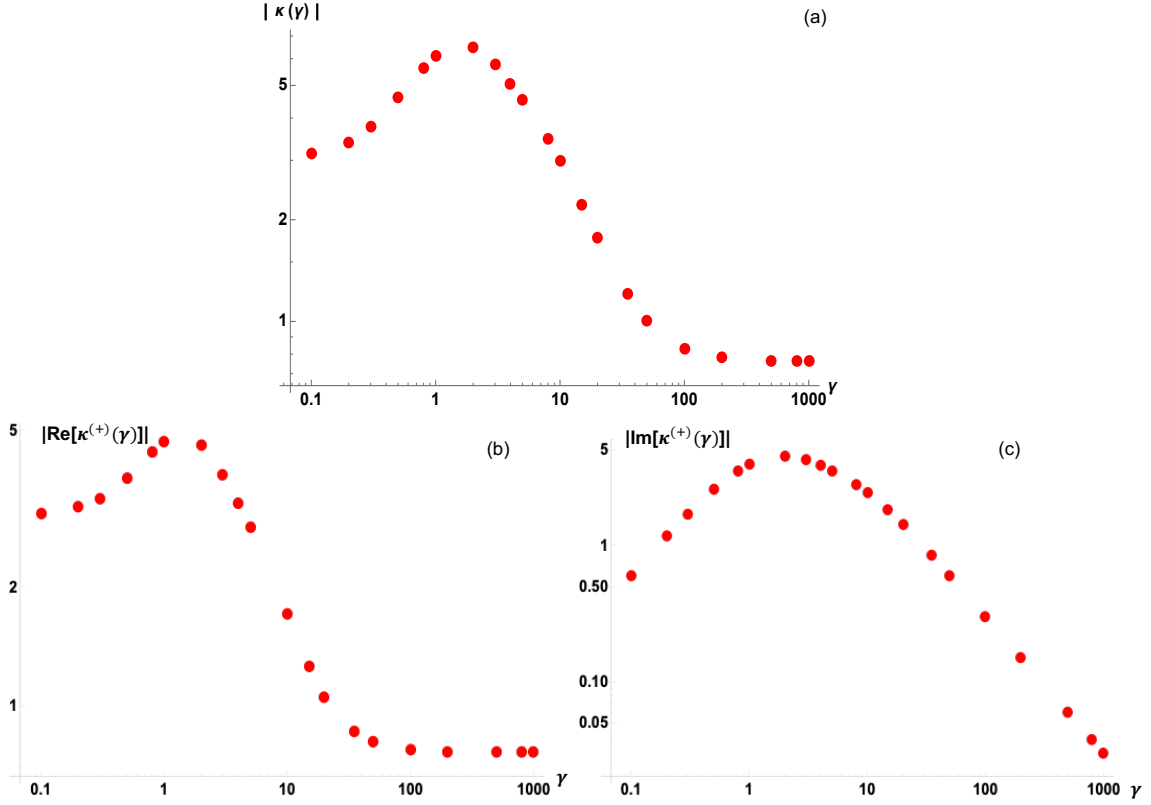


Figure 2. (a).A log-log plot of the specified list of γ and $|\kappa(\gamma)|$ values. (b). List log-log plot of γ and the absolute value of real part of $\kappa^{(+)}(\gamma)$. (c). List log-log plot of γ and the absolute value of the imaginary part of $\kappa^{(+)}(\gamma)$.

$\alpha^{(ab)(cd)}$ is a 10×10 matrix given by

$$\alpha^{(ab)(cd)} = \alpha_1 \delta^{(ab)(cd)} + \alpha_2 m^{(ab)(cd)} + \alpha_3 n^{(ab)(cd)}, \quad (5.4)$$

$\delta^{(ab)(cd)} = 1$ if $(ab) = (cd)$, $m^{(ab)(cd)} = 1$ if just two indices are the same, and $n^{(ab)(cd)} = 1$ if all four indices are different, and in all other cases these quantities vanish [29]. $\alpha_1, \alpha_2, \alpha_3$ are free parameters. We choose $\alpha_1 = 2, \alpha_2 = 3, \alpha_3 = 4$ in our computation. [16] shows that coherent spin-networks with $\alpha_2 = \alpha_3 = 0$ relates to Thiemann's coherent state [17].

The EPRL 4-simplex amplitude with coherent spin-network boundary sums A_v over j_{ab} weighted by $\psi_{j_0, \phi_0}(\vec{j})$. The 4-simplex amplitude for a coherent spin network state

$$\begin{aligned} A'_v &= \sum_{j_{ab} \in \mathbb{Z}_+/2 \cup \{0\}} \psi_{j_0, \phi_0}(\vec{j}) A_v(j_{ab}, i_a) \\ &= \sum_{j_{ab} \in \mathbb{Z}_+/2 \cup \{0\}} \int \prod_{a=2}^5 dg_a \int_{(\mathbb{C}\mathbb{P}^1)^{10}} e^{S_{\text{tot}}} \prod_{a < b} \frac{d_{j_{ab}}}{\pi} \Omega_{ab}, \end{aligned} \quad (5.5)$$

where the "total action" S_{tot} is given by

$$S_{\text{tot}}(j_{ab}, g, \mathbf{z}) = -\frac{1}{2} \sum_{ab, cd} \alpha^{(ab)(cd)} \frac{j_{ab} - (j_0)_{ab}}{\sqrt{(j_0)_{ab}}} \frac{j_{cd} - (j_0)_{cd}}{\sqrt{(j_0)_{cd}}} - i \sum_{ab} \gamma \phi_0^{ab} (j_{ab} - (j_0)_{ab}) + S(j, g, \mathbf{z}), \quad (5.6)$$

where S is the same action as in (2.4).

We use Poisson resummation formula

$$\sum_{j \in \mathbb{Z}_+ / 2 \cup \{0\}} f(j) = \frac{1}{2} \sum_{j \in \mathbb{Z} / 2} f(|j|) + \frac{1}{2} f(0) \quad (5.7)$$

$$= 2 \sum_{k \in \mathbb{Z}} \int_0^\infty dj f(j) e^{4\pi i k j} + \frac{1}{2} f(0) \quad (5.8)$$

where $f(j)$ corresponds to the summand in Eq.(5.5). When $(j_0)_{ab}$ are large, the gaussian in ψ_{j_0, ϕ_0} is peaked at large spins $j_{ab} = (j_0)_{ab}$. $|\psi_{j_0, \phi_0}|$ is exponentially small when j_{ab} is far from the large $(j_0)_{ab}$, so $f(0)$ is exponentially small and negligible. Similarly, the integral $\int dj$ is dominated by the large- j domain with $j_{ab} \sim (j_0)_{ab}$, while the integral outside this domain is exponentially suppressed. Motivated by this, we scale j_{ab} and $(j_0)_{ab}$ by $j_{ab} \rightarrow \lambda j_{ab}$ and $(j_0)_{ab} \rightarrow \lambda (j_0)_{ab}$. Therefore, "total action" is scaled by $S_{\text{tot}} \rightarrow \lambda S_{\text{tot}}$, and

$$A'_v = (2\lambda)^{10} \sum_{k_{ab} \in \mathbb{Z}} \int \prod_{a < b} dj_{ab} \frac{d\lambda j_{ab}}{\pi} \int \prod_{a=2}^5 dg_a \int_{(\mathbb{C}\mathbb{P}^1)^{10}} e^{\lambda S_{\text{tot}}^{(k)}} \prod_{a < b} \Omega_{ab} \quad (5.9)$$

where

$$S_{\text{tot}}^{(k)} = S_{\text{tot}} + 4\pi i \sum_{a < b} j_{ab} k_{ab} \quad (5.10)$$

Integrals in Eq.(5.9) can be analyzed with stationary phase approximation as in Theorem 2.1. Critical point equations of each $S_{\text{tot}}^{(k)}$ are

$$\text{Re}(S_{\text{tot}}) = 0, \quad \partial_{j_{ab}} S_{\text{tot}} = 4\pi i k_{ab}, \quad \partial_{g_a} S = \partial_{z_{ab}} S = 0. \quad (5.11)$$

It is not hard to see these equations implies critical equations of S in Eqs.(2.8) and $j_{ab} = (j_0)_{ab}$. Among 2 solutions $\vec{\mathbf{x}}_0^{(\pm)}$ of Eq.(2.8), only $\vec{\mathbf{x}}_0^{(+)}$ satisfy Eq.(5.11) when all $k_{ab} = 0$, because of Eqs.(5.3). Any $k_{ab} \neq 0$ leads to no solution for Eqs.(5.3). Therefore all integrals except for all $k_{ab} = 0$ in (5.9) are suppressed as $O(\lambda^{-N})$ for all positive integer N .

We focus on all $k_{ab} = 0$ and neglect exponentially small errors

$$\begin{aligned} A'_v &= (2\lambda)^{10} \int \prod_{a < b} dj_{ab} \left(\frac{d\lambda j_{ab}}{\pi} \right) \int \prod_{a=2}^5 dg_a \int_{(\mathbb{C}\mathbb{P}^1)^{10}} e^{\lambda S_{\text{tot}}} \prod_{a < b} \Omega_{ab} \\ &= (2\lambda)^{10} \int \prod_{i=1}^{54} d\eta_i u'(\boldsymbol{\eta}) e^{i\lambda \tilde{S}_{\text{tot}}(\boldsymbol{\eta})}, \quad \boldsymbol{\eta} = (\{j_{ab} - (j_0)_{ab}\}_{a < b}, \vec{\mathbf{x}}) \end{aligned} \quad (5.12)$$

where $\tilde{S}_{\text{tot}} = -iS_{\text{tot}}$ and $u'(\boldsymbol{\eta}) = u(\vec{\mathbf{x}}) \prod_{a < b} (d\lambda j_{ab} / \pi)$. The asymptotic expansion (2.7) can be applied to compute (5.12). As a difference from A_v , A'_v has only one critical point given by $j_{ab} = (j_0)_{ab}$ and $\vec{\mathbf{x}} = \vec{\mathbf{x}}_0^+$, because the boundary coherent spin-network specifies both boundary 3-geometry and extrinsic curvature [30].

5.2 Numerical results

The asymptotic expansion of A'_v with the next-to-leading order correction can be computed with the same scheme as in Section 4.2. Numerical results are presented below. Mathematica codes can be downloaded at [21].

As an example, at $\gamma = 0.1$,

$$A'_v = C'(\gamma) \left[1 + \frac{\kappa'(\gamma)}{\lambda} + O\left(\frac{1}{\lambda^2}\right) \right] \quad (5.13)$$

$$\begin{aligned}
&= 2^{10} \left(1 + \frac{1}{4\lambda}\right)^6 \left(1 + \frac{1}{10\lambda}\right)^4 \frac{1.85 \times 10^{-9} + 9.31 \times 10^{-10}i}{\lambda^7} e^{4.60\lambda i} \\
&\quad \left[1 + \frac{26.58 + 30.78i}{\lambda} + O\left(\frac{1}{\lambda^2}\right)\right], \tag{5.14}
\end{aligned}$$

where $C'(\gamma)$ stands for the leading order. $\kappa'(\gamma)$ is the next-to-leading order coefficient. The ratio of next-to-leading order corrections to leading-order term is

$$\frac{\kappa'(\gamma)}{\lambda} = \frac{1}{\lambda} \frac{I'(\gamma)}{u'(0)}, \tag{5.15}$$

here, $I' = I'_1 + I'_2 + I'_3$ is obtained by applying the computation in Eq.(4.8), (4.10) and (4.12) to u' and \tilde{S}_{tot} . $u'(0) = \frac{3.18}{2^{48}\pi^{26}}$ at the leading order is independent of γ .

From the result in Eq.(5.14), the next-to-leading order coefficient gives $|\kappa'(0.1)| \simeq 40.67$ at $\gamma = 0.1$. When $\lambda = 30$, $|\kappa'(0.1)/\lambda| \simeq 1.36$ is even greater than the leading order. Clearly the expansion in this case is invalid at $\lambda = 30$. The semiclassical approximation of A'_v (approximation by the leading order) requires a much larger λ . For example $\lambda \geq 300$ where $|\kappa'(0.1)/\lambda|$ is bounded by about 13% of the leading order. We suggest $\lambda \geq 3000$ to be a much better regime for A'_v at $\gamma = 0.1$ where the next-to-leading order is about 1% of the leading order.

The increase of allowed λ in A'_v may due to the increase of degrees of freedom (DOFs) by including the sum over j in A'_v . Therefore we expect that an even larger λ may be required to validate the large- j expansion for general spinfoam amplitudes on many 4-simplices with summing over internal spins.

Moreover, we study numerically the dependence of κ' on γ . We list some results of $|I'(\gamma)|$ and $|\kappa'(\gamma)|$ at different values of γ in Table 6. The plot of $|\kappa'(\gamma)|$ versus γ is given by Fig.(3).

Table 6. $|I'(\gamma)|$ and $|\kappa'(\gamma)|$ at different γ .

γ	0.1	0.5	1	2	3	4	5	8
$2^{48}\pi^{26} I'(\gamma) $	129.13	23.86	7.45	1.75	50.96	6.17	2.91	2.77
$ \kappa'(\gamma) $	40.67	7.51	2.34	0.55	16.05	1.94	0.92	0.87
γ	10	20	50	100	200	500	800	1000
$2^{48}\pi^{26} I'(\gamma) $	2.77	2.64	2.46	2.34	2.32	2.32	2.32	2.32
$ \kappa'(\gamma) $	0.87	0.83	0.77	0.75	0.74	0.73	0.73	0.73

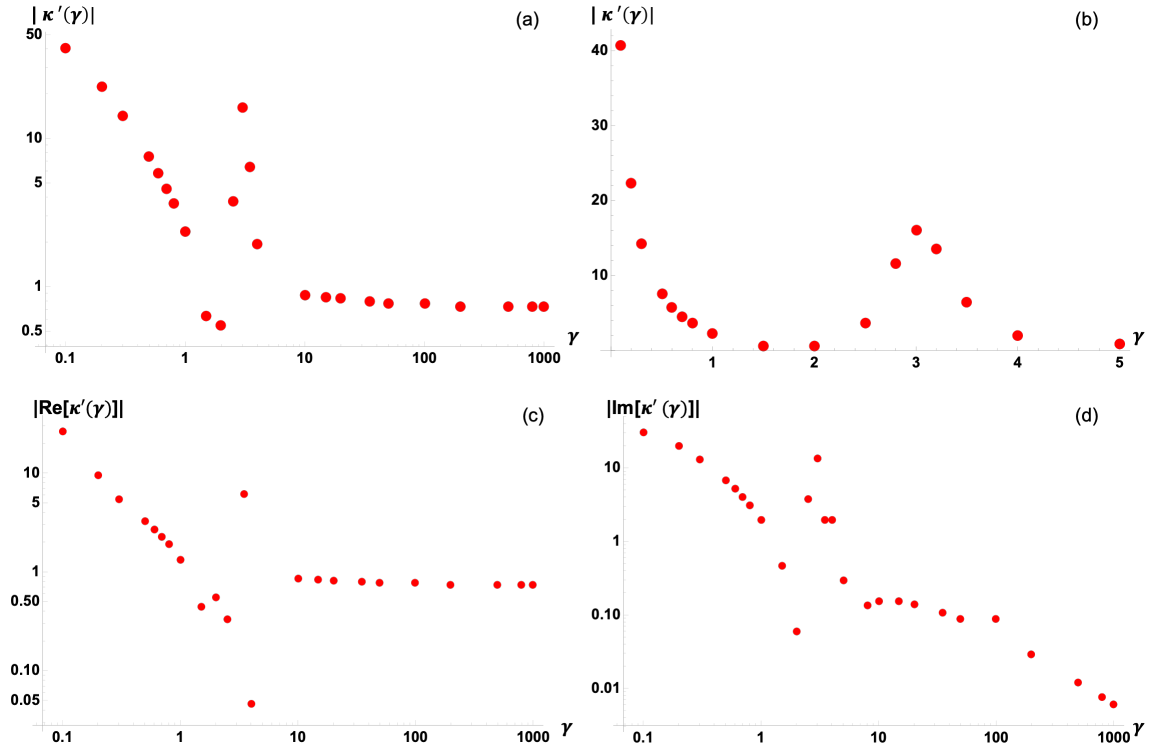


Figure 3. (a): The log-log plot of $|\kappa'(\gamma)|$ versus γ . (b): The plot of $|\kappa'(\gamma)|$ with relatively small γ . Panel (b) is a zoom of panel (a) for $\gamma \in [0.1, 5]$. (c) The log-log plot of the absolute value of the real part of $\kappa'(\gamma)$. (d): The log-log plot of absolute value of the imaginary part of $\kappa'(\gamma)$.

From Table 6 and Figure 3, we find the next-to-leading order corrections depend on γ . $|\kappa'(\gamma)|$ decreases first and then increase, there is a local maximum at around $\gamma = 3$. After that, it drops again. Figure 3 (c) and (d) indicate that $\kappa'(\gamma)$ stabilize to real constants 0.73 asymptotically as $\gamma \rightarrow \infty$.

6 Conclusion

In this paper, we use the coherent-intertwiner and coherent spin-network respectively as boundary states to study the large- j asymptotic expansion of the EPRL 4-simplex amplitude. We numerically derive the next-to-leading order corrections and compare them to the leading-order. We demonstrate how next-to-leading order correction depends on the Barbero-Immirzi parameter γ , and how to obtain quantum corrections to the Regge action. In the context of this, our work makes it possible to quantitatively describe the quantum behaviour of 4-Simplex model. We can also estimate a proper regime defined by λ where the semiclassical approximation of A_v is valid, with a dominate leading order term and a negligible next-to-leading order correction.

The future generalization of this work may be along two directions: spinfoam amplitudes with multiple 4-simplices and nonperturbative computations. The challenge of generalizing to multiple 4-simplices relates to increasing number of integration variables, which makes the computation in Section 4.2 more expensive. However, it may be still interesting and possible to study the complex with three 4-simplices as the model in [31] and understand how the next-to-leading order correction interacts with the issue of flatness in the spinfoam model.

The other direction is to numerically evaluate the spinfoam amplitude nonperturbatively (without the asymptotic expansion), in order to understand the model both in and beyond the large- j regime. It has been difficult since the integral e.g. (2.2) is oscillatory which makes numerical evaluation difficult. However, recent developments in lattice gauge theories discover new Monte-Carlo methods on Lefschetz thimbles for oscillatory integrals [32, 33]. The strategy is firstly deforming the integration contour to integration cycles called Lefschetz thimbles on which $\text{Im}(S)$ is a constant, then applying the Monte-Carlo simulation to non-oscillatory integrals on Lefschetz thimbles. We have applied this method to study the amplitude A'_v , and results will be reported elsewhere [34].

Acknowledgements

The authors acknowledge Pietro Dona, Giorgio Sarno, and Simone Speziale for helpful discussions. This work receives support from the National Science Foundation through grant PHY-1912278.

A The $\text{SL}(2, \mathbb{C})$ Haar measure

Here, we derive the $\text{SL}(2, \mathbb{C})$ Haar measure dg in our case.

For any $\text{SL}(2, \mathbb{C})$ group element, it can be parameterized as:

$$g = a_0 I + \sum_{k=1}^3 a_k \sigma_k = \begin{pmatrix} a_0 + a_3 & a_1 - ia_2 \\ a_1 + ia_2 & a_0 - a_3 \end{pmatrix} = \begin{pmatrix} \alpha & \beta \\ \gamma & \omega \end{pmatrix} = \begin{pmatrix} \alpha_1 + i\alpha_2 & \beta_1 + i\beta_2 \\ \gamma_1 + i\gamma_2 & \omega_1 + i\omega_2 \end{pmatrix}, \quad (\text{A.1})$$

here, I is 2×2 identity matrix, σ_k is Pauli matrix, and $a_i (i = 0, 1, 2, 3)$,

$$\alpha = \alpha_1 + i\alpha_2, \quad \beta = \beta_1 + i\beta_2,$$

$$\gamma = \gamma_1 + i\gamma_2, \quad \omega = \omega_1 + i\omega_2,$$

are complex variables, where $\alpha_1, \alpha_2, \beta_1, \beta_2, \gamma_1, \gamma_2, \omega_1, \omega_2$ are real.

From the book [35], the measure for the group $\text{SL}(2, \mathbb{C})$ is

$$\begin{aligned} dg &= c_0^2 \delta(a_0^2 - \sum_{k=1}^3 a_k^2 - 1) \prod_{i=0}^3 Da_i, \quad c_0 = \pi^{-2} \\ &= \frac{1}{\pi^4} \delta(a_0^2 - \sum_{k=1}^3 a_k^2 - 1) \left| \det \left(\frac{\partial (Re(a_0), Im(a_0), \dots, Re(a_3), Im(a_3))}{\partial (Re(\alpha_1), Im(\alpha_2), \dots, Re(\omega_1), Im(\omega_2))} \right) \right| D\alpha D\beta D\gamma D\omega \quad (\text{A.2}) \\ &= \frac{1}{16\pi^4} \delta(\alpha\omega - \gamma\beta - 1) D\alpha D\beta D\gamma D\omega, \end{aligned}$$

here, we use this calculation

$$\begin{aligned} a_0^2 - \sum_{k=1}^3 a_k^2 - 1 &= \alpha\omega - \gamma\beta - 1, \\ \det \left(\frac{\partial (Re(a_0), Im(a_0), \dots, Re(a_3), Im(a_3))}{\partial (Re(\alpha_1), Im(\alpha_2), \dots, Re(\omega_1), Im(\omega_2))} \right) &= \frac{1}{16}. \end{aligned}$$

One can find the details in our Mathematica notebooks [21]. For any complex variable $z = x + iy$, we use the notation:

$$Dz = dx dy \quad \text{and} \quad \delta(z) = \delta(x)\delta(y).$$

Then, (A.2) can be derived as

$$\begin{aligned} dg &= \frac{1}{16\pi^4} \delta(\alpha_1\omega_1 - \alpha_2\omega_2 - \beta_1\gamma_1 + \beta_2\gamma_2 - 1) \delta(\alpha_1\omega_2 + \alpha_2\omega_1 - \beta_1\gamma_2 - \beta_2\gamma_1) d\omega_1 d\omega_2 D\alpha D\beta D\gamma \\ &= \frac{1}{16\pi^4} \frac{D\alpha D\beta D\gamma}{|\alpha|^2} = \frac{1}{16\pi^4} \frac{d\alpha_1 d\alpha_2 d\beta_1 d\beta_2 d\gamma_1 d\gamma_2}{|\alpha|^2}. \end{aligned} \quad (\text{A.3})$$

The following calculation can show the details for the third step. For convenience, we define

$$\begin{aligned} f_1 &= \text{Re}(\alpha\omega - \gamma\beta - 1) = \alpha_1\omega_1 - \alpha_2\omega_2 - \beta_1\gamma_1 + \beta_2\gamma_2 - 1, \\ f_2 &= \text{Im}(\alpha\omega - \gamma\beta - 1) = \alpha_1\omega_2 + \alpha_2\omega_1 - \beta_1\gamma_2 - \beta_2\gamma_1. \end{aligned}$$

Then, the product of delta function can be written as

$$\delta(f_1)\delta(f_2) = \frac{\delta(\omega_1 - \hat{\omega}_1)\delta(\omega_2 - \hat{\omega}_2)}{\left| \det \frac{\partial(f_1, f_2)}{\partial(\omega_1, \omega_2)} \right|}, \quad \left| \det \frac{\partial(f_1, f_2)}{\partial(\omega_1, \omega_2)} \right| = \alpha_1^2 + \alpha_2^2 = |\alpha|^2,$$

here, $\hat{\omega}_1$ and $\hat{\omega}_2$ are the solutions of the system fo equations $f_1 = 0$ and $f_2 = 0$,

$$\begin{aligned} \hat{\omega}_1 &= \frac{\alpha_1 + \alpha_1\beta_1\gamma_1 + \alpha_2\beta_2\gamma_1 + \alpha_2\beta_1\gamma_2 - \alpha_1\beta_2\gamma_2}{\alpha_1^2 + \alpha_2^2}, \\ \hat{\omega}_2 &= \frac{\alpha_1(\beta_2\gamma_1 + \beta_1\gamma_2) + \alpha_2(-1 - \beta_1\gamma_1 + \beta_2\gamma_2)}{\alpha_1^2 + \alpha_2^2}. \end{aligned}$$

Next, we parametrized

$$\alpha = 1 + \frac{1}{\sqrt{2}}(x_1 + iy_1), \beta = \frac{1}{\sqrt{2}}(x_2 + iy_2), \gamma = \frac{1}{\sqrt{2}}(x_3 + iy_3).$$

i.e.,

$$\alpha_1 = 1 + \frac{x_1}{\sqrt{2}}, \alpha_2 = \frac{y_1}{\sqrt{2}}, \beta_1 = \frac{x_2}{\sqrt{2}}, \beta_2 = \frac{y_2}{\sqrt{2}}, \gamma_1 = \frac{x_3}{\sqrt{2}}, \gamma_2 = \frac{y_3}{\sqrt{2}}.$$

Then, (A.3) can be written as

$$dg = \frac{1}{16\pi^4 \times 2^3} \frac{dx_1 dy_1 dx_2 dy_2 dx_3 dy_3}{\left| 1 + \frac{x_1 + iy_1}{\sqrt{2}} \right|^2}, \quad (\text{A.4})$$

which is the $\text{SL}(2, \mathbb{C})$ group haar measure we used in our case. The parameters of the $\text{SL}(2, \mathbb{C})$ group are

$$g = \begin{pmatrix} 1 + \frac{x_1 + iy_1}{\sqrt{2}} & \frac{x_2 + iy_2}{\sqrt{2}} \\ \frac{x_3 + iy_3}{\sqrt{2}} & \frac{1 + \frac{x_2 + iy_2}{\sqrt{2}} \frac{x_3 + iy_3}{\sqrt{2}}}{1 + \frac{x_1 + iy_1}{\sqrt{2}}} \end{pmatrix}. \quad (\text{A.5})$$

At the critical point $g = \mathbb{1}$ or $\vec{x} = \vec{y} = 0$,

$$dg \rightarrow \frac{1}{16\pi^4 \times 2^3} dx_1 dy_1 dx_2 dy_2 dx_3 dy_3. \quad (\text{A.6})$$

References

- [1] T. Thiemann, *Modern Canonical Quantum General Relativity*. Cambridge Monographs on Mathematical Physics. Cambridge University Press, 2007.
- [2] A. Ashtekar and J. Lewandowski, *Background independent quantum gravity: A Status report*, *Class.Quant.Grav.* **21** (2004) R53, [[gr-qc/0404018](#)].

- [3] M. Han, W. Huang, and Y. Ma, *Fundamental structure of loop quantum gravity*, *Int. J. Mod. Phys. D* **16** (2007) 1397–1474, [[gr-qc/0509064](#)].
- [4] C. Rovelli and F. Vidotto, *Covariant Loop Quantum Gravity: An Elementary Introduction to Quantum Gravity and Spinfoam Theory*. Cambridge Monographs on Mathematical Physics. Cambridge University Press, 2014.
- [5] A. Perez, *The Spin Foam Approach to Quantum Gravity*, *Living Rev. Rel.* **16** (2013) 3, [[arXiv:1205.2019](#)].
- [6] J. Engle, E. Livine, R. Pereira, and C. Rovelli, *LQG vertex with finite Immirzi parameter*, *Nucl. Phys. B* **799** (2008) 136–149, [[arXiv:0711.0146](#)].
- [7] C. Rovelli, *Simple model for quantum general relativity from loop quantum gravity*, *J. Phys. Conf. Ser.* **314** (2011) 012006, [[arXiv:1010.1939](#)].
- [8] J. W. Barrett, R. J. Dowdall, W. J. Fairbairn, F. Hellmann, and R. Pereira, *Lorentzian spin foam amplitudes: Graphical calculus and asymptotics*, *Class. Quant. Grav.* **27** (2010) 165009, [[arXiv:0907.2440](#)].
- [9] M. Han and M. Zhang, *Asymptotics of Spinfoam Amplitude on Simplicial Manifold: Lorentzian Theory*, *Class. Quant. Grav.* **30** (2013) 165012, [[arXiv:1109.0499](#)].
- [10] F. Conrady and L. Freidel, *Path integral representation of spin foam models of 4d gravity*, *Class. Quant. Grav.* **25** (2008) 245010, [[arXiv:0806.4640](#)].
- [11] M. Han and T. Krajewski, *Path Integral Representation of Lorentzian Spinfoam Model, Asymptotics, and Simplicial Geometries*, *Class. Quant. Grav.* **31** (2014) 015009, [[arXiv:1304.5626](#)].
- [12] E. R. Livine and S. Speziale, *A New spinfoam vertex for quantum gravity*, *Phys. Rev.* **D76** (2007) 084028, [[arXiv:0705.0674](#)].
- [13] E. Bianchi, L. Modesto, C. Rovelli, and S. Speziale, *Graviton propagator in loop quantum gravity*, *Class. Quant. Grav.* **23** (2006) 6989–7028, [[gr-qc/0604044](#)].
- [14] E. Bianchi, E. Magliaro, and C. Perini, *LQG propagator from the new spin foams*, *Nucl. Phys.* **B822** (2009) 245–269, [[arXiv:0905.4082](#)].
- [15] E. Bianchi and Y. Ding, *Lorentzian spinfoam propagator*, *Phys. Rev.* **D86** (2012) 104040, [[arXiv:1109.6538](#)].
- [16] E. Bianchi, E. Magliaro, and C. Perini, *Coherent spin-networks*, *Phys. Rev.* **D82** (2010) 024012, [[arXiv:0912.4054](#)].
- [17] T. Thiemann, *Gauge field theory coherent states (GCS): 1. General properties*, *Class. Quant. Grav.* **18** (2001) 2025–2064, [[hep-th/0005233](#)].
- [18] P. Dona, M. Fanizza, G. Sarno, and S. Speziale, *Numerical study of the Lorentzian Engle-Pereira-Rovelli-Livine spin foam amplitude*, *Phys. Rev.* **D100** (2019), no. 10 106003, [[arXiv:1903.12624](#)].
- [19] L. Hormander, *The Analysis of Linear Partial Differential Operators I*. Springer-Verlag Berlin, 1983.
- [20] V. Bonzom, E. R. Livine, M. Smerlak, and S. Speziale, *Towards the graviton from spinfoams: The Complete perturbative expansion of the 3d toy model*, *Nucl. Phys. B* **804** (2008) 507–526, [[arXiv:0802.3983](#)].
- [21] M. Han, Z. Huang, H. Liu, and D. Qu. <https://github.com/dqu2017/Numerical-Asymptotics>, 2020.
- [22] P. Dona and G. Sarno, *Numerical methods for EPRL spin foam transition amplitudes and Lorentzian recoupling theory*, *Gen. Rel. Grav.* **50** (2018) 127, [[arXiv:1807.03066](#)].
- [23] B. Bahr and S. Steinhaus, *Numerical evidence for a phase transition in 4d spin foam quantum gravity*, *Phys. Rev. Lett.* **117** (2016), no. 14 141302, [[arXiv:1605.07649](#)].

- [24] B. Bahr, G. Rabuffo, and S. Steinhaus, *Renormalization of symmetry restricted spin foam models with curvature in the asymptotic regime*, *Phys. Rev. D* **98** (2018), no. 10 106026, [[arXiv:1804.00023](#)].
- [25] F. Conrady and L. Freidel, *On the semiclassical limit of 4d spin foam models*, *Phys. Rev.* **D78** (2008) 104023, [[arXiv:0809.2280](#)].
- [26] J. W. Barrett, R. J. Dowdall, W. J. Fairbairn, H. Gomes, and F. Hellmann, *Asymptotic analysis of the EPRL four-simplex amplitude*, *J. Math. Phys.* **50** (2009) 112504, [[arXiv:0902.1170](#)].
- [27] M.-X. Han and M. Zhang, *Asymptotics of Spinfoam Amplitude on Simplicial Manifold: Euclidean Theory*, *Class. Quant. Grav.* **29** (2012) 165004, [[arXiv:1109.0500](#)].
- [28] L. Freidel and K. Krasnov, *A New Spin Foam Model for 4d Gravity*, *Class. Quant. Grav.* **25** (2008) 125018, [[arXiv:0708.1595](#)].
- [29] C. Rovelli, *Graviton propagator from background-independent quantum gravity*, *Phys. Rev. Lett.* **97** (2006) 151301, [[gr-qc/0508124](#)].
- [30] E. Bianchi, E. Magliaro, and C. Perini, *Spinfoams in the holomorphic representation*, *Phys. Rev. D* **82** (2010) 124031, [[arXiv:1004.4550](#)].
- [31] P. Dona, F. Gozzini, and G. Sarno, *Numerical analysis of spin foam dynamics and the flatness problem*, [arXiv:2004.12911](#).
- [32] E. Witten, *Analytic Continuation Of Chern-Simons Theory*, *AMS/IP Stud. Adv. Math.* **50** (2011) 347–446, [[arXiv:1001.2933](#)].
- [33] P. F. Bedaque, *A complex path around the sign problem*, *EPJ Web Conf.* **175** (2018) 01020, [[arXiv:1711.05868](#)].
- [34] M. Han, Z. Huang, H. Liu, and D. Qu, *Monte-Carlo simulation of spinfoam amplitude on Lefschetz thimble*, to appear.
- [35] W. Ruhl, *The Lorentz group and harmonic analysis*. W.A. Benjamin, 1970.